J. Fluid Mech. (2012), *vol.* 711, *pp.* 122–146.
doi:10.1017/jfm.2012.380

Reynolds number effects on lipid vesicles

David Salac[1]† **and Michael J. Miksis**[2]

[1] Department of Mechanical and Aerospace Engineering, University at Buffalo SUNY, Buffalo, NY 14260, USA

[2] Engineering Sciences and Applied Mathematics, Northwestern University, Evanston, IL 60208, USA

(Received 10 November 2011; revised 7 May 2012; accepted 23 July 2012; first published online 31 August 2012)

Vesicles exposed to the human circulatory system experience a wide range of flows and Reynolds numbers. Previous investigations of vesicles in fluid flow have focused on the Stokes flow regime. In this work the influence of inertia on the dynamics of a vesicle in a shearing flow is investigated using a novel level-set computational method in two dimensions. A detailed analysis of the behaviour of a single vesicle at finite Reynolds number is presented. At low Reynolds numbers the results recover vesicle behaviour previously observed for Stokes flow. At moderate Reynolds numbers the classical tumbling behaviour of highly viscous vesicles is no longer observed. Instead, the vesicle is observed to tank-tread, with an equilibrium angle dependent on the Reynolds number and the reduced area of the vesicle. It is shown that a vesicle with an inner/outer fluid viscosity ratio as high as 200 will not tumble if the Reynolds number is as low as 10. A new damped tank-treading behaviour, where the vesicle will briefly oscillate about the equilibrium inclination angle, is also observed. This behaviour is explained by an investigation on the torque acting on a vesicle in shear flow. Scaling laws for vesicles in inertial flows have also been determined. It is observed that quantities such as vesicle tumbling period follow square-root scaling with respect to the Reynolds number. Finally, the maximum tension as a function of the Reynolds number is also determined. It is observed that, as the Reynolds number increases, the maximum tension on the vesicle membrane also increases. This could play a role in the creation of stable pores in vesicle membranes or for the premature destruction of vesicles exposed to the human circulatory system.

Key words: capsule/cell dynamics, membranes, multiphase flow

1. Introduction

Vesicles have been proposed in various biotechnologies, such as drug delivery systems (Choon & Cullis 1995; Allen & Cullis 2004; Torchilin 2006). Vesicles used in such a technology would be exposed to all conditions in the circulatory system, from creeping flow (Fung & Zweifach 1971) to flows where inertia cannot be ignored (Ku *et al.* 1985). As a result, the behaviour of vesicles in external flows has been of great interest experimentally (Abkarian, Lartigue & Viallat 2002; Abkarian & Viallat 2005, 2008; Abkarian, Faivre & Viallat 2007; Coupier *et al.* 2008; Deschamps *et al.* 2009*a*; Deschamps, Kantsler & Steinberg 2009*b*), theoretically (Vlahovska & Gracia 2007; Lebedev, Turitsyn & Vergeles 2008; Danker, Vlahovska & Misbah 2009; Vlahovska, Podgorski & Misbah 2009; Schwalbe, Vlahovska & Miksis 2010) and

† Email address for correspondence: davidsal@buffalo.edu

numerically (Du, Liu & Wang 2006; Misbah 2006; Du & Zhang 2008; Du *et al.* 2009; Veerapaneni *et al.* 2009*a*,*b*). In the Stokes flow regime, two major behaviours have been observed. The first is a tank-treading motion, where a vesicle's orientation remains constant in time while the membrane rotates (Lebedev *et al.* 2008; Deschamps *et al.* 2009*a*; Veerapaneni *et al.* 2009*b*). The second is classified as tumbling, where an end-over-end rotation of the vesicle is observed (Seifert 1997; Kantsler & Steinberg 2006; Lebedev *et al.* 2008). A third regime has recently been observed, described as either trembling (Lebedev *et al.* 2008; Zhao & Shaqfeh 2009, 2011) or breathing (Vlahovska & Gracia 2007). This third regime is an intermediate step between the tank-treading and tumbling cases. In the Stokes regime, a vesicle will transition from tank-treading to tumbling with an increase in the viscosity ratio between the encapsulated and external fluid (Kantsler & Steinberg 2006). Dependence on other parameters, such as density, has not been observed. Here we consider the effect of inertia on the dynamics of vesicles.

Flows at higher Reynolds number can occur in a number of situations. For example, consider the formation of clots in an artery, atherothrombosis. The highest shear rate typically found in normal circulation can reach 4700 s^{-1} (Tangelder *et al.* 1988). For a vesicle with a radius of 4 μm and typical blood fluid properties, this results in a shear Reynolds number of 0.02. If an artery is restricted due to a clot, then numerical studies have shown that the shear rate can increase to 84 000 s^{-1} (Strony *et al.* 1993) or even to peaks of 425 000 s^{-1} (Bark & Ku 2010), resulting in a Reynolds number of the order of 2. An understanding of how a vesicle drug delivery system behaves under such conditions is necessary to advance the technology.

As another example, consider ventricular assist devices. These are mechanical devices that augment or replace the function of one or more chambers of a failing heart. Device types include centrifugal, axial and pulsatile pump designs. Maximum Reynolds number in these devices range from 3321 in pulsatile pumps to 155 320 for centrifugal pumps (Fraser *et al.* 2011). Owing to the unphysiological conditions in circulatory systems using these devices, a wide range of blood damage can occur, including damage to erythrocytes, called haemolysis (Siegenthaler *et al.* 2002; Heilmann *et al.* 2009). In haemolysis, haemoglobin is released into the plasma due to mechanical compromise of the erythrocyte membrane. The mechanism for haemoglobin release may be the rupture of the cell (Rand 1964) or the formation of pores appearing in the cell membrane (Zhao *et al.* 2006). Vesicles form a model system for red blood cells (Noguchi, Gompper & Lubensky 2005; Abkarian & Viallat 2008), and knowledge of how these model systems respond to various flows will provide insight into the behaviour of red blood cells.

Recently Salac & Miksis (2010, 2011) presented a numerical method to model vesicle behaviour in finite-Reynolds-number flows. The method was a level-set computational scheme using a novel projection method. In that previous work, it was shown that a vesicle that should be tumbling in a viscous flow will tank-tread when the Reynolds number is increased. More recently Laadhari, Saramito & Misbah (2012) have observed similar behaviour.

Here we will use an extension of the computational approach of Salac & Miksis (2011) to provide a systematic numerical investigation of the dynamics of vesicles in flows where both inertial and viscous effects are important. A parameter study will be presented showing how inertial effects result in the vesicle transitioning from the tumbling back to the tank-treading regime as the Reynolds number varies. The existence of this critical Reynolds number agrees with work dealing with rigid particles in inertial flow (Zettner & Yoda 2001; Mikulencack & Morris 2004).

The physical problem, including a short description of the mathematical formulation, and the numerical method are presented in § 2. Verification of the method and a discussion of the validity of using a two-dimensional computation to model three-dimensional vesicles is presented in § 3. Numerical results for a single vesicle in simple inertial shear flow are presented in § 4. A systematic investigation of vesicle behaviour in inertial flows, including relevant scaling laws, is shown in § 5. A discussion, including a comparison with rigid particles in inertial shear flows, follows in § 6. Finally, in § 7 a brief conclusion and possible future work are presented.

2. Problem description and numerical method

Consider a single vesicle suspended in a fluid. This vesicle encapsulates another fluid with known properties that may differ from those of the surrounding fluid. Under general flow conditions, the system is governed by the full Navier–Stokes equations with interfacial boundary conditions on the vesicle membrane. It is assumed that the velocity field is continuous across the membrane and the stress has a jump in the normal direction proportional to the force per unit area acting on the membrane. To enforce surface incompressibility, the velocity at the interface must also be surface-divergence-free, $\boldsymbol{\nabla}_s \cdot \boldsymbol{u} = 0$.

The force per unit area on the membrane can be derived from the free energy of the membrane and is equal to $b_n(\nabla_s^2\kappa + \frac{1}{2}\kappa^3)\boldsymbol{n} - \gamma\kappa\boldsymbol{n} + \boldsymbol{\nabla}_s\gamma\boldsymbol{s}$, with a bending rigidity of b_n, an interfacial mean curvature of κ, and a spatially varying tension-like parameter γ. Here $\boldsymbol{s}$ represents the tangential vector and $\nabla_s^2 = \boldsymbol{\nabla}_s \cdot \boldsymbol{\nabla}_s$ is the surface Laplacian.

The present study is based on level-set tracking of the vesicle membrane and a projection method for the fluid equations (Salac & Miksis 2011). The location of the vesicle is implicitly determined by an auxiliary mathematical function $\phi(\boldsymbol{x}, t)$, where $\boldsymbol{x}$ is a position in space. The vesicle membrane at time t is taken to be $\Gamma(t) = \{\boldsymbol{x} : \phi(\boldsymbol{x}, t) = 0\}$. It is assumed that $\phi(\boldsymbol{x}, t) < 0$ corresponds to the region enclosed by the membrane. Material parameters such as density and viscosity can be calculated at any point by $f(\boldsymbol{x}, t) = f_{in} + (f_{out} - f_{in})H(\phi(\boldsymbol{x}, t))$, where f is the material quantity needed and $H(y)$ is the Heaviside function such that $H(y) = 0$ for $y < 0$ and $H(y) = 1$ for $y \geqslant 0$.

Let a two-dimensional vesicle of encapsulated area A have a membrane length of L. A characteristic length is defined as $R_0 = L/2\pi$, while velocity is characterized by $u_0 = \dot{\gamma}R_0$. A vesicle is characterized by a reduced area parameter, $\nu = A/(\pi R_0^2) = 4\pi A/L^2$, which relates the encapsulated area of a vesicle to that of a circle with the same membrane length. If a characteristic pressure and tension are defined as $p_0 = \dot{\gamma}\mu_{out}$ and $\gamma_0 = \dot{\gamma}R_0\mu_{out}$, where μ_{out} is the viscosity of the external fluid, then two dimensionless quantities can be determined. The first is the shear Reynolds number, $Re = \rho_{out}\dot{\gamma}R_0^2/\mu_{out}$, while the second is a capillary bending number, $Ca = R_0^3\mu_{out}\dot{\gamma}/b_n$. The capillary bending number relates the strength of applied shear flow to the bending energy. The density and viscosity are normalized with respect to the external fluid values. A single Navier–Stokes equation valid in the entire domain can be calculated as (Salac & Miksis 2011):

$$\rho\frac{\mathrm{D}\boldsymbol{u}}{\mathrm{D}t} = -\frac{1}{Re}\boldsymbol{\nabla}p + \frac{1}{Re}\boldsymbol{\nabla}\cdot(\mu(\boldsymbol{\nabla}\boldsymbol{u} + \boldsymbol{\nabla}^{\mathrm{T}}\boldsymbol{u})) + \frac{1}{Re}\delta(\phi)(|\boldsymbol{\nabla}\phi|\boldsymbol{\nabla}_s\gamma - \gamma\kappa\boldsymbol{\nabla}\phi) + \frac{1}{CaRe}\delta(\phi)\left(\nabla_s^2\kappa + \frac{1}{2}\kappa^3\right)\boldsymbol{\nabla}\phi, \tag{2.1}$$

where $\delta(\phi)$ is the Dirac delta function given by $\delta(y) = \mathrm{d}H(y)/\mathrm{d}y$.

2.1. *Numerical method*

The method used in this study is an extension of the previous method developed by Salac & Miksis (2011). Changes from the original method are presented below.

The fluid field is solved using a second-order in time and space lagged pressure–tension semi-Lagrangian projection method. The semi-Lagrangian component is based on the work of Xiu & Karniadakis (2001) while the lagged pressure and tension are based on the work of Brown, Cortez & Minion (2001). This method represents an improvement on the previous work of Salac & Miksis (2011). To advance the fluid field from a time t^n to a time $t^{n+1} = t^n + \Delta t$, it is assumed that the velocity at times t^{n-2}, t^{n-1} and t^n are known. The lagged pressure $p^{n-1/2}$ and tension $\gamma^{n-1/2}$ are also known.

The first step is a semi-implicit velocity approximation given by

$$\begin{aligned}\rho\frac{3\boldsymbol{u}^* - 4\boldsymbol{u}_d^n + \boldsymbol{u}_d^{n-1}}{2\Delta t} = &-\frac{1}{Re}\nabla p^{n-1/2} + \frac{1}{Re}\nabla\cdot\left(\mu\left(\nabla\boldsymbol{u}^* + \left(\nabla\hat{\boldsymbol{u}}^{n+1}\right)^{\mathrm{T}}\right)\right)\\ &+\frac{1}{ReCa}\left(\nabla_s^2\kappa + \frac{1}{2}\kappa^3\right)\delta(\phi)\nabla\phi\\ &+\frac{1}{Re}\delta(\phi)\left(\nabla_s\gamma^{n-1/2} - \gamma^{n-1/2}\kappa\boldsymbol{n}\right),\end{aligned} \tag{2.2}$$

where $\boldsymbol{u}_d^n$ and $\boldsymbol{u}_d^{n-1}$ are the departure velocities at times t^n and t^{n-1}. The quantity $\hat{\boldsymbol{u}}^{n+1}$ is a second-order approximation to the true velocity field $\boldsymbol{u}^{n+1}$. Standard second-order extrapolation resulted in unstable oscillations of the fluid field in certain situations. To avoid this instability, the approximate velocity is defined as $\hat{\boldsymbol{u}}^{n+1} = \boldsymbol{u}^n + \mathrm{minmod}(\boldsymbol{u}^n - \boldsymbol{u}^{n-1}, \boldsymbol{u}^{n-1} - \boldsymbol{u}^{n-2})$, where $\mathrm{minmod}(x, y)$ equals 0 if $xy < 0$, x if $|x| < |y|$, and y otherwise.

The next step is a pressure and tension correction step:

$$\rho\frac{\boldsymbol{u}^{n+1} - \boldsymbol{u}^*}{\Delta t} = -\frac{1}{Re}\nabla\hat{p} + \frac{1}{Re}\delta(\phi)(\nabla_s\hat{\gamma} - \hat{\gamma}\kappa\boldsymbol{n}) \tag{2.3}$$

subject to the constraints $\nabla\cdot\boldsymbol{u}^{n+1} = 0$ in Ω and $\nabla_s\cdot\boldsymbol{u}^{n+1}$ on Γ. This equation is solved using an iterative technique to enforce both conditions. The pressure and tension for the next iteration are given by $p^{n+1/2} = p^{n-1/2} + 3\hat{p}/2$ and $\gamma^{n+1/2} = \gamma^{n-1/2} + 3\hat{\gamma}/2$. Using this correction form, the pressure and tension are at least first-order accurate, ensuring that the velocity field is second order (Brown *et al.* 2001).

All results presented will be for a single vesicle with the same density as the exterior fluid. The vesicle is contained in a square computational domain of size $2L$ centred at the origin. The goal is to investigate inertial effects on vesicle behaviour, and thus ideally the vesicle would be in an infinite domain. To approximate this condition, the velocity boundary conditions on the domain are periodic in the x direction and Dirichlet velocity boundary conditions of $\boldsymbol{u} = (\pm L, 0)$ in the y direction. A confinement parameter is introduced as $h = R_0/L$, where R_0 is the radius of a circular vesicle with the same membrane length. Unless otherwise stated, all results will be obtained using a confinement parameter of $h = 1/5$.

The simulations are solved on an adaptive non-graded Cartesian grid (Min & Gibou 2006, 2007) using a maximum grid spacing 0.156 25 and a minimum grid spacing of 0.0390 625 with a uniform time step of 0.001. In all cases the enclosed area and membrane length have been tracked. These quantities never deviate from their initial values by more than 0.1 %. All of the simulations are started by assuming zero

pressure, zero tension and an initial velocity field of $\boldsymbol{u}_0 = (y, 0)$. The simulation is then run for 50 iterations while keeping the vesicle stationary to obtain an initial pressure, tension and velocity field.

Inclination angles are determined by calculating the eigenvalues and eigenvectors of the vesicle's inertia tensor about its centre of mass. The eigenvector corresponding to the larger of the two eigenvalues provides the direction of the long axis of a vesicle. In the following, inclination angles are reported as the angle of the the vesicle in the right half of the domain and the positive x axis. This results in the angle having values between $-\pi$ and $+\pi$. A jump will be seen when the angle of the vesicle becomes lower than $-\pi$, as the angle will now be measured with respect to the opposite tip. Vesicles will also be described by a deformation parameter given by $D = (L - B)/(L + B)$, where L and B are the long and short axes of an ellipse with the same inertia tensor (Ramanujan & Pozrikidis 1998).

3. Verification and influence of confinement

In this section, verification of the numerical method and the influence of confinement will be presented. The verification will be compared to both two- and three-dimensional results. It will be shown that, despite being a two-dimensional simulation, the results correctly predict the behaviour of three-dimensional vesicles. It will also be seen that confinement of the domain plays an important part in the behaviour of vesicles in inertial flows.

3.1. *Verification of the method*

To validate the method, results from the present scheme are compared to available Stokes flow results. First, consider vesicles ranging from a reduced area of $\nu = 0.6$ to $\nu = 0.9$, all with a unit viscosity ratio, $\eta = 1$, placed in a simple shear flow described by $Re = 10^{-3}$ and $Ca = 100$. It is known that the vesicle will reach an equilibrium inclination angle with respect to the flow direction. The equilibrium inclination angle using the scheme presented above has been measured and compared to the work of Kraus *et al.* (1996), Kantsler & Steinberg (2006) and Veerapaneni *et al.* (2009*b*). To compare with the three-dimensional experimental results of Kantsler & Steinberg (2006), it is first necessary to convert the reduced volume of a three-dimensional vesicle into a reduced area of a two-dimensional vesicle. This is accomplished by considering the maximum section in the shear plane of a three-dimensional vesicle under shear flow and then calculating the reduced area of this shear plane (Ghigliotti, Biben & Misbah 2010). Using both numerical (Zhao & Shaqfeh 2009) and experimental (Kantsler & Steinberg 2005; Zabusky *et al.* 2011) three-dimensional data, the relationship $\nu = \nu_V^{1.639}$ has been determined, where ν is the two-dimensional reduced area used here and ν_V is the three-dimensional reduced volume. The result for the equilibrium angle is seen in figure 1. The two-dimensional results of this work agree well with previous two-dimensional numerical and three-dimensional experimental results.

At equilibrium, a tank-treading vesicle with $\eta = 1$ will obtain a constant shape. This shape can be described by the deformation parameter D described above. For three-dimensional vesicles it has been predicted that the parameter D scales as $\sqrt{\Delta}$, where Δ is the excess area of a vesicle (Seifert 1999). In two dimensions the parameter Δ is the excess interfacial length and is related to the reduced area by $\Delta = 2(1 - \sqrt{\nu})/(\pi\sqrt{\nu})$. Using the method outlined above, the deformation parameter

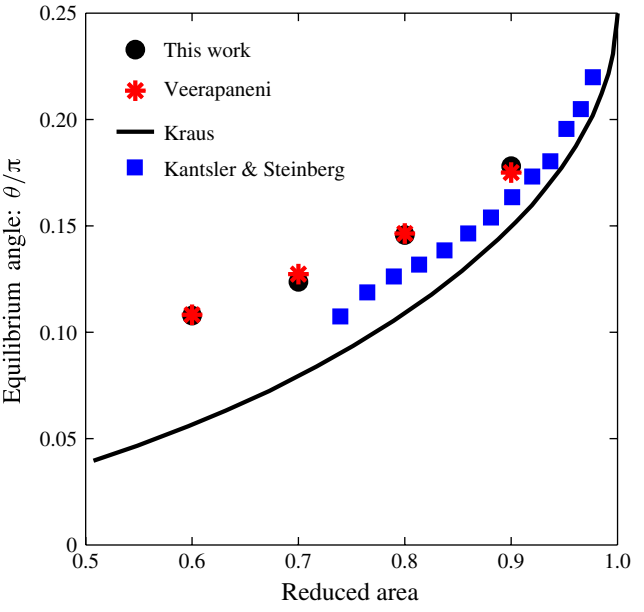

FIGURE 1. (Colour online) The equilibrium inclination angle for various vesicles in simple shear flow with $\eta = 1$, $Re = 10^{-3}$ and $Ca = 100$. The result is compared to previously published results of Kraus *et al.* (1996) and Veerapaneni *et al.* (2009*b*) and the experimental results of Kantsler & Steinberg (2006).

for a tank-treading vesicle is shown as a function of excess length in figure 2. As can be seen, the deformation parameter scales as predicted.

As the viscosity ratio increases, it is known that a vesicle in simple shear flow will transition from the tank-treading regime to the tumbling regime. The viscosity ratio required for this transition has been determined for various vesicles in shear flow described by $Re = 10^{-3}$ and $Ca = 100$. The result is compared to the analytic result of Keller & Skalak (1982) and the experimental result of Kantsler & Steinberg (2006) using the reduced volume–reduced area conversion above. The comparison is seen in figure 3. The behaviour of the present method compares well to both the analytic method and experimental results. This result, in addition to the results shown in figures 1 and 2, demonstrates that the two-dimensional results presented here predict the correct behaviour.

3.2. *Influence of confinement*

To explore the influence of the computational domain on the behaviour of the vesicle, a study has been performed using a single vesicle with a reduced area of $v = 0.7$ under the conditions of $Re = 10^{-3}$ and $Ca = 100$ with various confinement levels. First, consider a vesicle with no viscosity contrast, $\eta = 1$, placing the vesicle in the tank-treading regime. The behaviour of the vesicle for varying levels of confinement are shown in figure 4. It appears that, at confinement levels greater than $h = 1/4$, the influence of the boundary begins to be minimized.

If the viscosity contrast is increased to $\eta = 8$, the vesicle will now be in the tumbling regime. The dynamic behaviour of the vesicle for various confinement levels

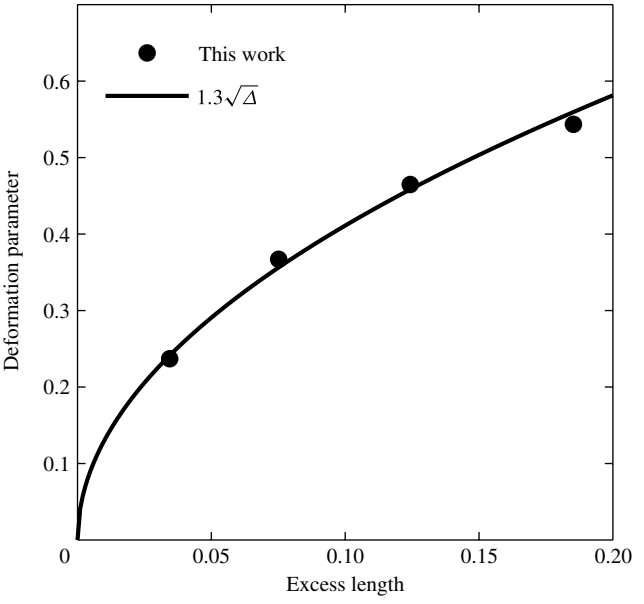

FIGURE 2. The deformation parameter, D, at equilibrium versus the vesicle excess length, Δ, during tank-treading in simple shear flow with $\eta = 1$, $Re = 10^{-3}$ and $Ca = 100$. The deformation scales as $\sqrt{\Delta}$ as shown by Seifert (1999).

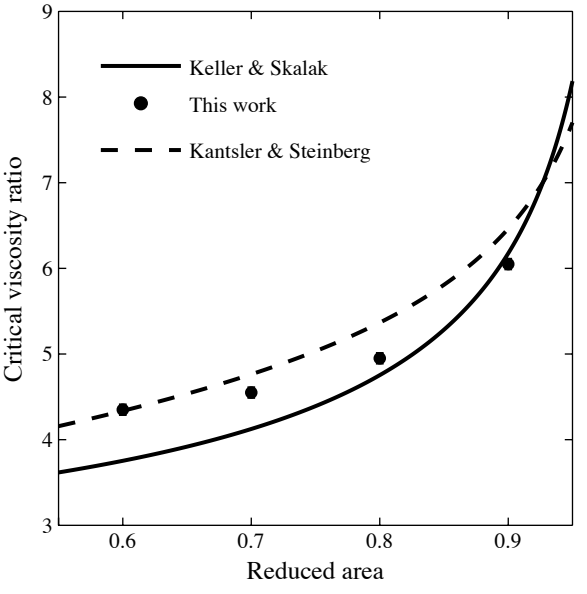

FIGURE 3. The viscosity ratio required to transition from the tank-treading to tumbling regimes for vesicles with various reduced areas in a flow described by $Re = 10^{-3}$ and $Ca = 100$. The result is compared to the analytic work of Keller & Skalak (1982) and the experimental results of Kantsler & Steinberg (2006).

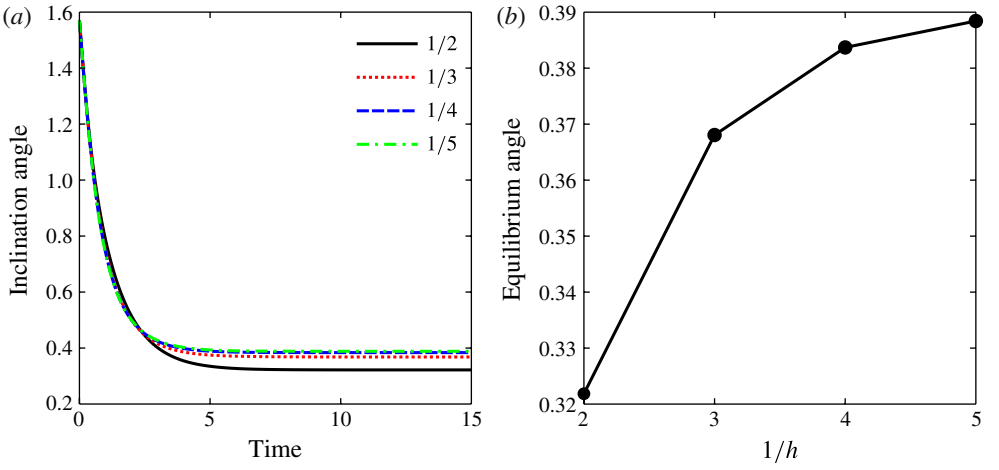

FIGURE 4. (Colour online) Influence of the confinement on the behaviour of a tank-treading vesicle given by $\nu = 0.7$ and $\eta = 1$ with $Re = 10^{-3}$ and $Ca = 100$. (*a*) The inclination angle of the vesicle over time for values of h from $1/2$ to $1/5$. (*b*) The equilibrium inclination angle versus confinement level.

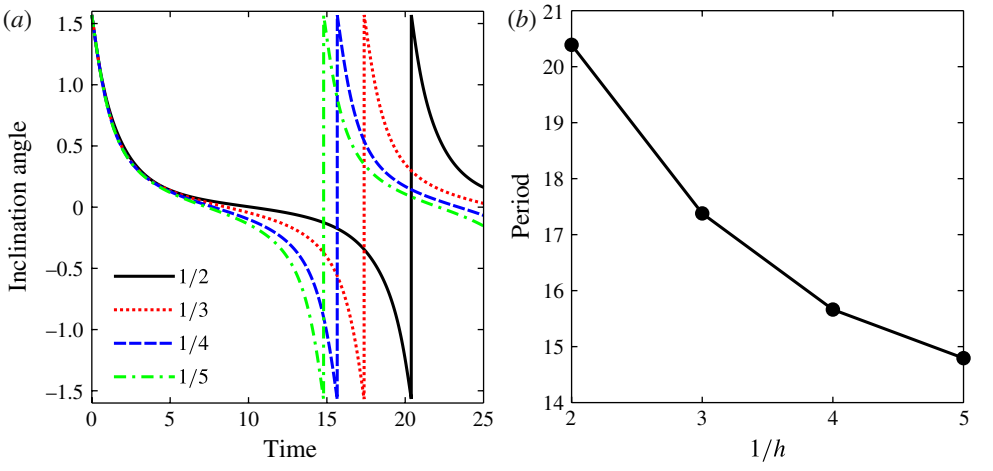

FIGURE 5. (Colour online) Influence of the confinement on the behaviour of a tumbling vesicle given by $\nu = 0.7$ and $\eta = 8$ with $Re = 10^{-3}$ and $Ca = 100$. (*a*) The inclination angle of the vesicle over time for values of h from $1/2$ to $1/5$. (*b*) The tumbling period versus confinement level.

under these conditions is given in figure 5. As before, the influence of the boundaries begins to diminish for confinement levels greater than $h = 1/4$.

The need for a low confinement level can be further demonstrated by considering the same vesicle with a reduced area of $\nu = 0.7$ and viscosity ratio $\eta = 20$ in a flow described by $Re = 2$ and $Ca = 100$. This vesicle is placed in two computational domains. The first is a domain of size $[-2, 2] \times [-2, 2]$, giving a confinement value of $h = 1/2$ in both directions. The second is a domain of size $[-5, 5] \times [-2, 2]$, giving a confinement value of $1/5$ in the x direction and $1/2$ in the y direction. As the domain

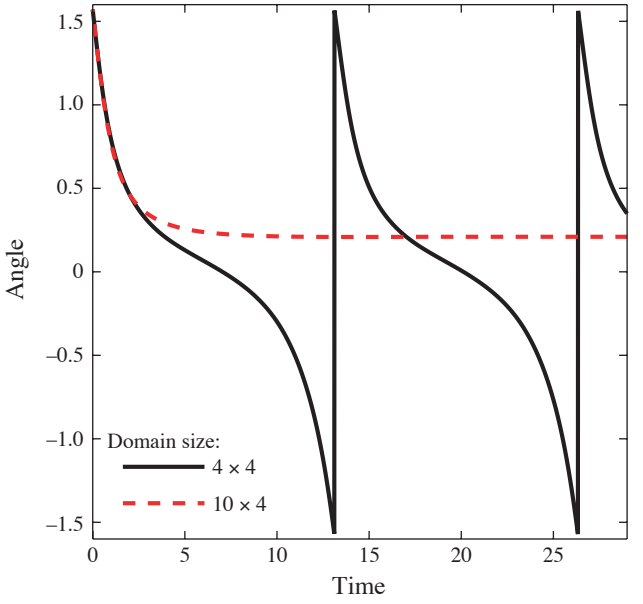

FIGURE 6. (Colour online) Inclination angle of a vesicle described by $\nu = 0.7$ and $\eta = 20$ in a flow with $Re = 2$ and $Ca = 100$ for two computational domains of $[-5, 5] \times [-2, 2]$ and $[-2, 2] \times [-2, 2]$. The influence of the boundary conditions in the x direction for the smaller domain is clearly demonstrated.

sizes are the same in the y direction, any change in behaviour will be due solely to the boundary conditions enforced in the x direction. The resulting behaviour of the vesicle over time is shown in figure 6. Clearly, the behaviour of the vesicle is drastically altered by the utilization of a small computational domain. Based on the results of this section, and to avoid any overt influence of boundary conditions on the results, a uniform confinement level of $h = 1/5$ is chosen for the remaining results.

4. Inertial effects on a vesicle with $\nu = 0.7$

To explore the influence of inertia on the behaviour of vesicles this section will consider a single vesicle with a reduced area of $\nu = 0.7$ and a capillary number of $Ca = 100$. We begin by setting the viscosity ratio to $\eta = 10$. In viscous flows, this is firmly in the tumbling regime – see figure 3. The inclination angle and deformation of the vesicle over time in various Reynolds number flows are shown in figure 7. An increase in the Reynolds number results in a longer tumbling period. Above a critical Reynolds number, the vesicle no longer tumbles and returns to the tank-treading behaviour. Additionally, it appears that the maximum change in the deformation parameter increases as the Reynolds number increases. A detailed look at this vesicle and the fluid field for Reynolds numbers of 0.1 and 1.0 is presented in figure 8. The lower-Reynolds-number flow demonstrates the classical tumbling motion, while the higher-Reynolds-number flow clearly shows the tank-treading behaviour. An example of this transition was briefly mentioned in Salac & Miksis (2011). Preliminary results were also presented by the authors at the 63rd Annual Meeting of the APS Division of Fluid Dynamics (Salac & Miksis 2010).

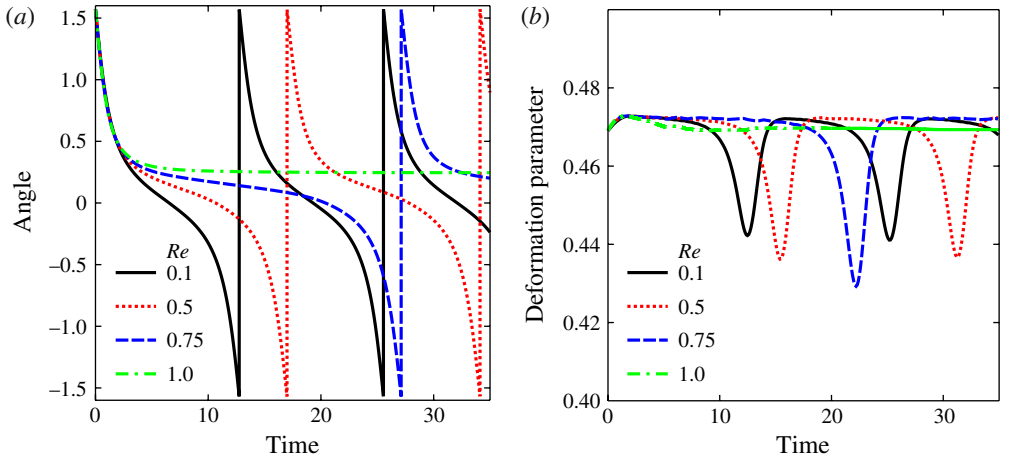

FIGURE 7. (Colour online) (*a*) Inclination angle and (*b*) deformation of a vesicle with reduced area of $\nu = 0.7$ and viscosity ratio of $\eta = 10$ with $Ca = 100$ and various Reynolds numbers. As the Reynolds number increases, the vesicle transitions from the tumbling regime back to a tank-treading state.

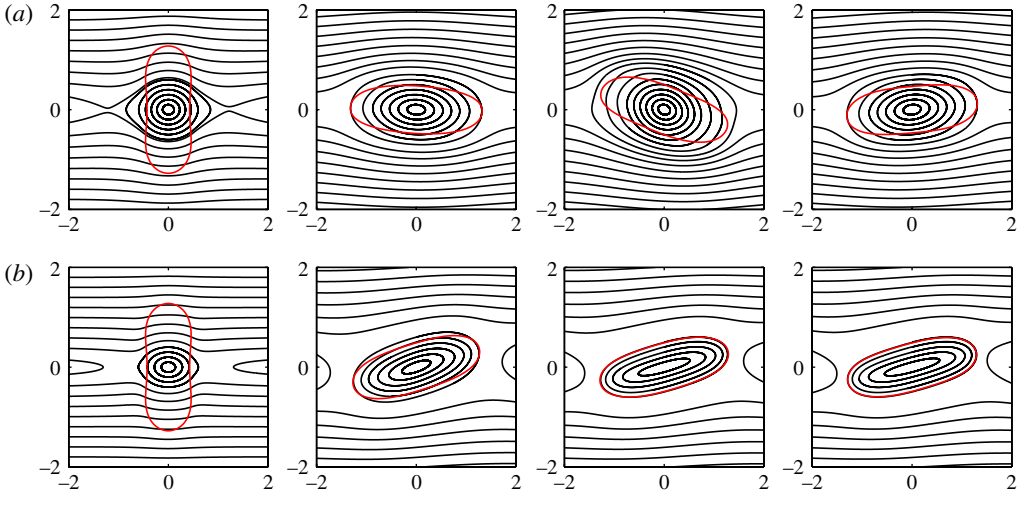

FIGURE 8. (Colour online) Dynamic behaviour of a vesicle with reduced area of $\nu = 0.7$ and viscosity ratio of $\eta = 10$ with $Ca = 100$ at times of $t = 0$, 5, 10, 20 for Reynolds numbers *Re* of (*a*) 0.1 and (*b*) 1.0.

The tumbling period for a vesicle with reduced area of $\nu = 0.7$ as a function of Reynolds number is shown in figure 9 for viscosity ratios from 10 to 80. Initially, the tumbling period only increases slightly as the Reynolds increases. As the Reynolds number approaches the critical Reynolds number, the tumbling period increases dramatically. As will be seen in § 5, the tumbling period obeys an inverse square-root scaling with respect to the Reynolds number.

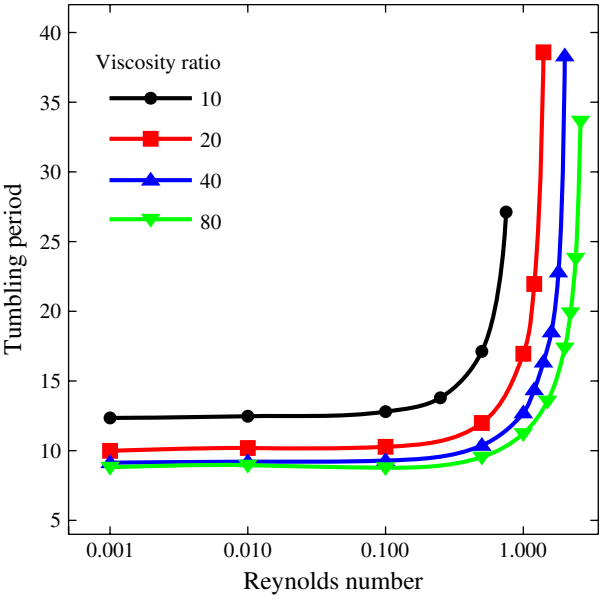

FIGURE 9. (Colour online) The tumbling period versus Reynolds number for a vesicle with reduced area $\nu = 0.7$ and various viscosity ratios. The tumbling period grows slowly until the Reynolds number approaches the critical Reynolds number, and then increases dramatically.

The influence of the Reynolds number and viscosity on the equilibrium angle of a vesicle with reduced area of $\nu = 0.7$ is presented in figure 10. For a given viscosity ratio, an increase in the Reynolds number results in an increase in the equilibrium tank-treading angle. For a given Reynolds number, an increase in the viscosity ratio results in a decrease in the equilibrium inclination angle. From these results there exists a maximum equilibrium inclination angle possible. Any further increase in Reynolds number would only result in slightly higher angles.

To verify the equilibrium angles observed at elevated Reynolds numbers, a vesicle with a reduced area of $\nu = 0.7$ and a viscosity ratio of $\eta = 10$ is started with inclination angles of $\theta_0 = 0$, 0.1, 0.2 and π. The inclination angle and deformation parameter versus time for a shear flow characterized by $Re = 1$ are given in figure 11. For the vesicles starting at initial angles of $\theta_0 = 0$ and $\theta_0 = 0.1$, a partial tumbling is observed, while for $\theta_0 = 0.2$ no tumbling is observed. In all cases the final equilibrium angle and deformation parameter match those of the vesicle starting vertically, $\theta_0 = \pi$. To further demonstrate the partial tumbling observed, the evolution of a vesicle with an initial angle of 0 is shown in figure 12. The partial tumbling and final equilibrium shape are clearly demonstrated.

Increasing the Reynolds number provides a further stabilizing influence, as seen in figure 13. Here the same vesicle is considered as in figure 11, with $\nu = 0.7$ and $\eta = 10$. This vesicle is placed in flow with a Reynolds number of $Re = 5$. Four major observations can be made. First, the equilibrium inclination angle for the $Re = 5$ case is larger than for the $Re = 1$ case, matching the result seen in figure 10. Second, the equilibrium deformation parameter appears to remain constant despite an increase in the Reynolds number. This behaviour is further explored in the next section. Third, no partial tumbling is observed, even in the initially horizontal vesicle. Finally, the behaviour of the vesicle demonstrates a damped tank-treading behaviour, where the

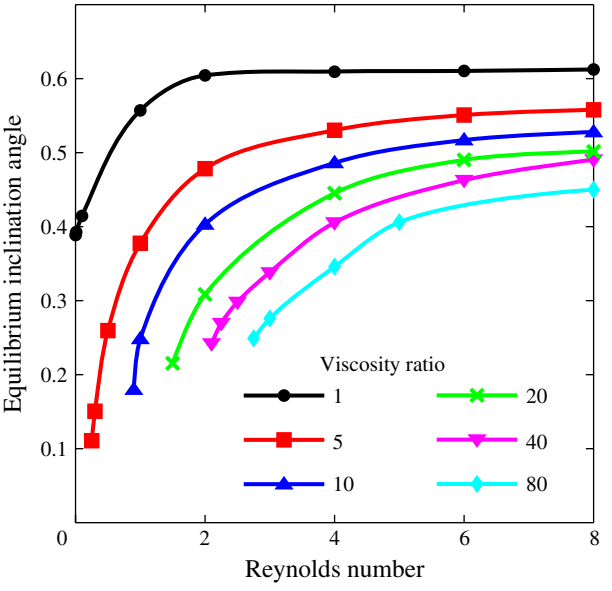

FIGURE 10. (Colour online) The equilibrium angle of a vesicle described by $\nu = 0.7$ with various viscosity ratios in flows given by $Ca = 100$ and various Reynolds numbers.

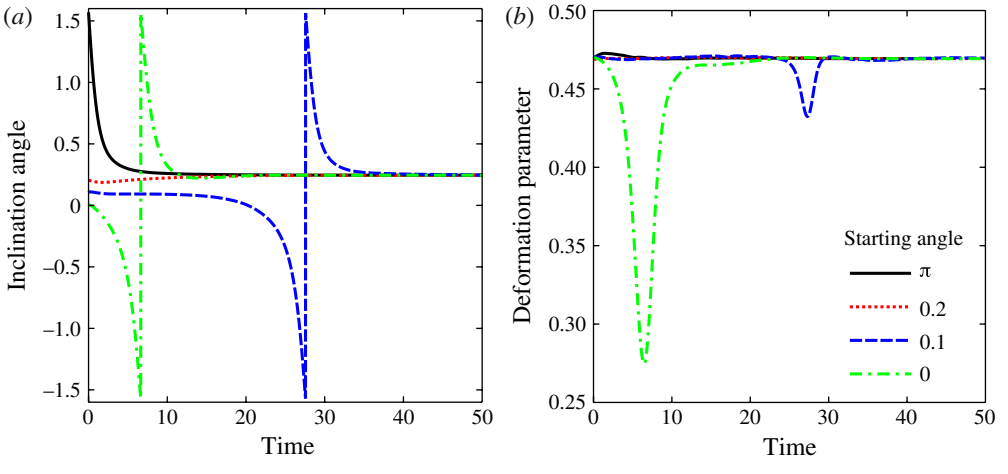

FIGURE 11. (Colour online) (*a*) Inclination angle and (*b*) deformation of a vesicle described by $\nu = 0.7$ and $\eta = 10$ in a flow given by $Ca = 100$ and $Re = 1$ for various initial starting angles.

vesicle rotates past the equilibrium angle and then returns. This damped tank-treading will also be further explored in § 6.

The tumbling behaviour of extremely high-viscosity-ratio vesicles can also be suppressed using only moderate Reynolds numbers, as seen in figure 14, where the response of a $\nu = 0.7$ vesicle with $\eta = 200$ is shown for a flow given by $Re = 10$ and $Ca = 100$. Even at this extremely high viscosity ratio, the vesicle will not tumble.

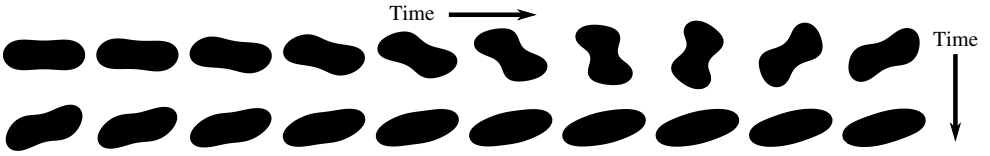

FIGURE 12. Snapshots of the vesicle shape for the $\theta_0 = 0$ case in figure 11. The snapshots are in time increments of 1 and begin in the upper left corner, with time increasing to the right and down.

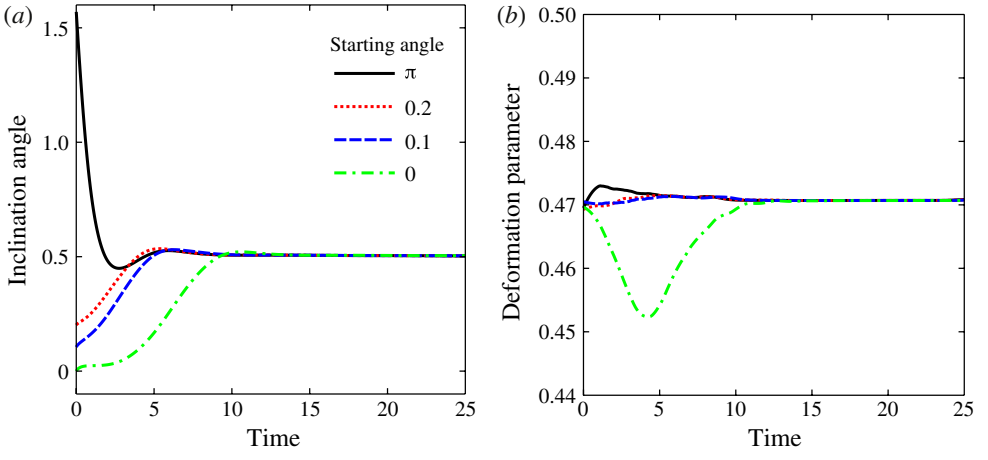

FIGURE 13. (Colour online) (*a*) Inclination angle and (*b*) deformation of a vesicle described by $\nu = 0.7$ and $\eta = 10$ in a flow given by $Ca = 100$ and $Re = 5$ for various initial starting angles.

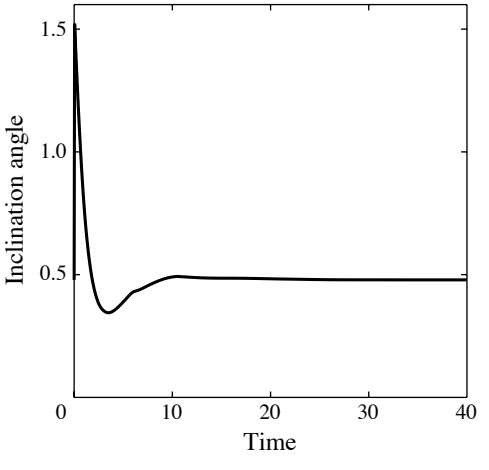

FIGURE 14. The angle of a vesicle described by $\nu = 0.7$ and $\eta = 200$ in a flow given by $Ca = 100$ and $Re = 10$.

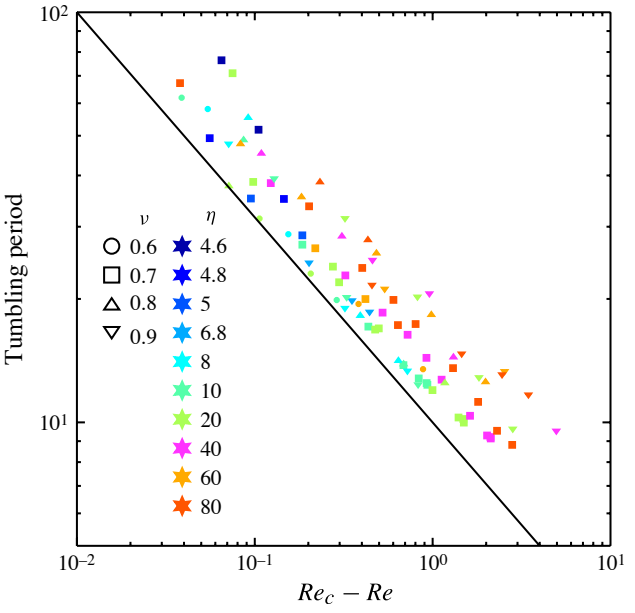

FIGURE 15. (Colour online) Log–log plot of the tumbling period as a function of the difference between the actual and critical Reynolds numbers for vesicles of various reduced areas and viscosity ratios. The symbol shapes indicate the reduced area, ν, of the vesicle, while the colours represent the viscosity ratio, η. The solid line corresponds to a scaling of $(Re_c - Re)^{-1/2}$.

5. A systematic investigation of vesicle behavior in inertial flows

This section will explore the generalized behaviour of vesicles in inertial flows. This is done by systematically considering the behaviour of four characteristic vesicles given by $\nu = 0.6$, 0.7, 0.8 and 0.9, with viscosity ratios ranging from $\eta = 1$ to $\eta = 80$. The range of Reynolds numbers considered here will be from $Re \approx 10^{-2}$ to $Re = 10$.

First, consider the tumbling period of vesicles below the critical Reynolds number. The tumbling period for a range of vesicles as a function of $Re_c - Re$, where Re_c is the critical Reynolds number for a given vesicle, is plotted in figure 15. In all cases, a tumbling vesicle observes a large increase in the tumbling period as the Reynolds number approaches the critical value (see figure 9 for an unscaled example). Similar to rigid particles in inertial flows (Ding & Aidun 2000; Zettner & Yoda 2001; Mikulencack & Morris 2004), it is observed that the tumbling period, GT, is related to the Reynolds number by

$$GT \propto (Re_c - Re)^{-1/2}. \tag{5.1}$$

It was suggested by Ding & Aidun (2000) that this type of scaling is valid for all rigid particles, independent of the particle shape. The results shown here demonstrate that this scaling also holds for deformable bodies where the surface area is held fixed. The $-1/2$ exponent in the scaling also indicates that vesicles undergo a saddle-node bifurcation as the Reynolds number increases, since the oscillation period scales to this exponent for any saddle-node bifurcation (Lichtenberg & Lieberman 1992).

Next, consider the critical Reynolds number for the tumbling to tank-treading transition. An exact critical Reynolds number is difficult to obtain, as a vesicle that

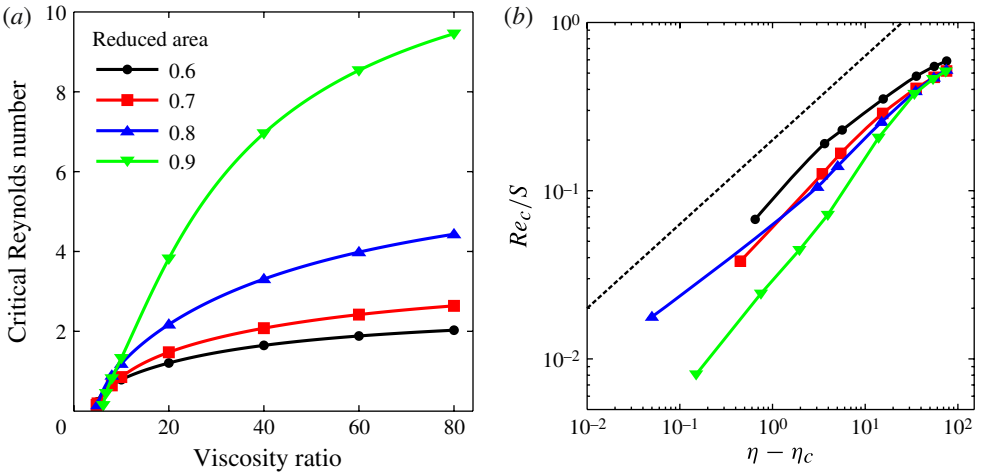

FIGURE 16. (Colour online) (*a*) The critical Reynolds number as a function of the viscosity ratio for vesicles ranging from $\nu = 0.6$ to $\nu = 0.9$. The results are shown with a confidence of ± 0.05. For any given vesicle, the region below the curve is the tumbling regime, while the region above the curve is the tank-treading regime. (*b*) Log–log plot of the critical Reynolds number normalized by the parameter S as a function of the viscosity ratio for four reduced areas. The dashed line corresponds to a scaling of $Re_c/S \propto (\eta - \eta_c)^{1/2}$.

appears to be tank-treading could actually be tumbling with an extremely large period. Based on the results shown in figure 9, the critical Reynolds number is estimated as the highest Reynolds number for which a vesicle will tumble within 100 units of time. Clearly this is only valid for vesicles with viscosity ratios greater than the Stokes flow critical viscosity ratio. The unscaled results are presented in figure 16(*a*). The critical Reynolds number results are shown with a confidence of ± 0.05. The region below these curves is the tumbling regime, while above the curves a vesicle would be tank-treading.

Several observations can be made. First, even for vesicles with high reduced area and high viscosity ratios, only moderate Reynolds numbers, less than $Re = 10$, are needed to stabilize a vesicle. Second, as the viscosity ratio increases, then so does the critical Reynolds number. Finally, for a given viscosity ratio, the critical Reynolds number depends on the reduced area, as vesicles with higher reduced areas have higher critical Reynolds numbers. This last point is similar to the general trend seen in viscous flows regarding the critical viscosity ratio associated with the transition from tank-treading to tumbling.

To determine how the critical Reynolds number varies with the viscosity ratio, a new parameter is introduced, $S = Ca\sqrt{\nu}/(100(1 - \sqrt{\nu}))$. This parameter behaves similarly to the parameter $7\pi Ca/(3\sqrt{3}\Delta)$, where Δ is the excess area parameter, used in investigations of three-dimensional vesicles in viscous flows (Lebedev *et al.* 2008; Deschamps *et al.* 2009*b*). In both cases the parameter is a measure of the strength of the shear flow compared to the bending of the vesicle. The critical Reynolds number normalized by S is plotted against the difference between the viscosity ratio and the critical viscosity ratio for the tank-treading/tumbling transition in Stokes flow, $\eta - \eta_c$. The result is seen in figure 16(*b*). Using this scaling it is observed that

$$Re_c \propto S\,(\eta - \eta_c)^{1/2}\,. \tag{5.2}$$

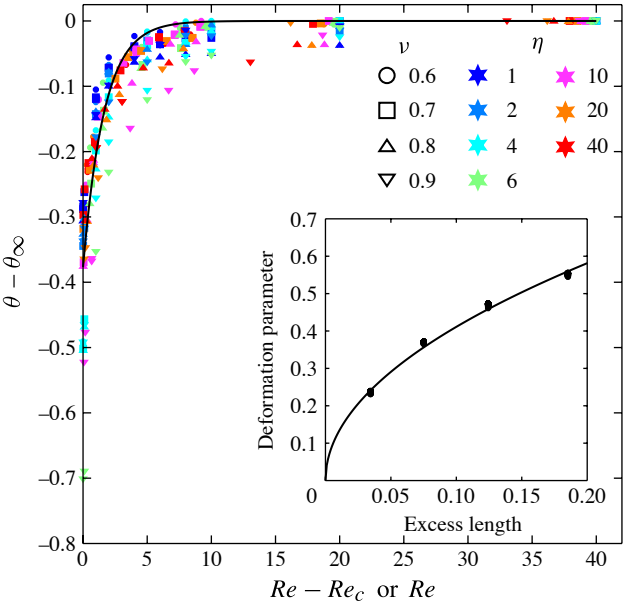

FIGURE 17. (Colour online) The difference between the final equilibrium angle and the actual equilibrium angle as a function of $Re - Re_c$, where Re_c is the critical Reynolds number for the tumbling to tank-treading transition if $\eta > \eta_c$ and $Re_c = 0$ if $\eta < \eta_c$. The symbol shapes indicate the reduced area, ν, of the vesicle, while the colours represent the viscosity ratio, η. The solid line corresponds to exponential decay with the equation $\theta = \theta_\infty - 0.377\exp[-0.605(Re - Re_c)]$. In this case the final equilibrium angle was taken to be the angle at $Re = 40$. Inset: The deformation parameter of the same vesicles. For the cases considered, the deformation at equilibrium still scales at $\sqrt{\Delta}$, where Δ is the excess length.

As is seen in figure 10, the equilibrium angle of a vesicle approaches a constant value with increasing Reynolds number. In figure 17 the difference between the equilibrium angle, θ, and the maximum equilibrium angle, θ_∞, is shown versus $Re - Re_c$, where Re_c is the critical Reynolds number for a given vesicle. For the case where the viscosity ratio is below the viscous critical viscosity ratio, then $Re_c = 0$. Using the combined data, exponential decay of the form

$$\theta = \theta_\infty - 0.377\mathrm{e}^{-0.605(Re - Re_c)} \tag{5.3}$$

is observed for all vesicles.

The deformation parameter for tank-treading vesicles at elevated Reynolds numbers is shown in the inset of figure 17. As in the viscous-dominated result seen in figure 2, the deformation parameter scales as $\sqrt{\Delta}$, regardless of the Reynolds number. This behaviour should be expected in the tank-treading regime. During tank-treading the forces exerted on the vesicle by the surrounding fluid are at a minimum. The bending energy will drive the vesicle towards a more energetically favourable configuration. It should be expected that the strength of the bending energy, denoted by the parameter Ca, will most probably play a role in the final inclination angle but not the equilibrium deformation. This will be explored in future research.

6. Discussion

6.1. *The total torque on a vesicle*

The results shown above bear a striking resemblance to work performed using rigid elliptical particles in inertial flows, both experimental (Zettner & Yoda 2001) and numerical (Ding & Aidun 2000; Mikulencack & Morris 2004). In these previous works, rigid elliptical particle of various sizes were studied in simple inertial shear flows. At low Reynolds numbers these particles would tumble end over end, similar to a vesicle. As the Reynolds number was increased, the rigid particles obtained an equilibrium angle with respect to the shear flow direction. This critical Reynolds number was of the order of $Re = 10$ and found to depend on the aspect ratio of the rigid particle. Despite the differences between rigid particle and flexible vesicles, namely that vesicles can dissipate energy through shape changes while rigid particles cannot, vesicles in finite-Reynolds-number flows observe the same scalings as rigid particles. This is due to the fact that the membrane length is fixed and we considered relatively stiff vesicles. Therefore, rigid particles may provide insight into the vesicle behaviour seen here.

It was suggested that the total torque acting on a rigid particle may provide insight into the counter-intuitive behaviour seen as the influence of inertia increases. The work of Ding & Aidun (2000) and Mikulencack & Morris (2004) demonstrated that, for rigid particles in flows above the critical Reynolds number, there existed torque-free conditions at certain inclination angles that matched the observed equilibrium angles. To explore this possibility, a sample vesicle described by $\nu = 0.7$ and $Ca = 100$ is placed in flows characterized by $Re = 0.1$ and $Re = 5$. Viscosity ratios of $\eta = 5$ and $\eta = 10$ are considered. For a vesicle undergoing motion, the total torque is calculated as

$$T_{net} = \int_{\Omega} (1 - H(\phi))(\boldsymbol{r} \times \boldsymbol{F}) \cdot \boldsymbol{e}_z \, \mathrm{d}A, \tag{6.1}$$

where $\boldsymbol{r}$ is the vector from the vesicle centre of mass to a point, $\boldsymbol{e}_z = (0, 0, 1)$ is the unit normal in the z direction and $\boldsymbol{F} = \mathrm{D}\boldsymbol{u}/\mathrm{D}t$ is the force being applied to a point. The integral is performed over the entire computational domain. The $1 - H(\phi)$ term ensures that only the region enclosed by the vesicle membrane has a contribution to the overall torque. In this formulation, a positive torque represents a net force rotating the vesicle in the anticlockwise direction (an increase in the angle).

The inclination angle and torque response of the $Re = 0.1$ and $\nu = 10$ case are shown in figure 18. Overall, the vesicle will tumble with a period of approximately 12.75. Initially, the vesicle has a positive net torque, which slows down the rotation rate. As the vesicle passes through the horizontal axis, a net negative torque is observed, accelerating the rotation rate in the clockwise direction. As the vesicle nears the $\theta = \pi$ (vertical) orientation, a large jump in the torque results in the vesicle decelerating.

Next consider the $Re = 5$ and $\nu = 10$ case. Unlike the $Re = 0.1$ situation, this vesicle will not tumble but instead reaches a stable inclination angle of approximately $\theta = 0.5$. Owing to the higher inertia, the vesicle rotates past the equilibrium angle, reaching a minimum angle of $\theta = 0.45$, before achieving equilibrium. The net torque is enough to reverse the angular velocity of the vesicle. As the vesicle rotates past the equilibrium angle, a net negative torque drives it to the final state.

In general, the forces exerted on a vesicle will rotate the vesicle. The tank-treading angle can be understood as the configuration where the net torque acting on the vesicle is zero. For a vesicle to remain at an inclination angle other than the equilibrium

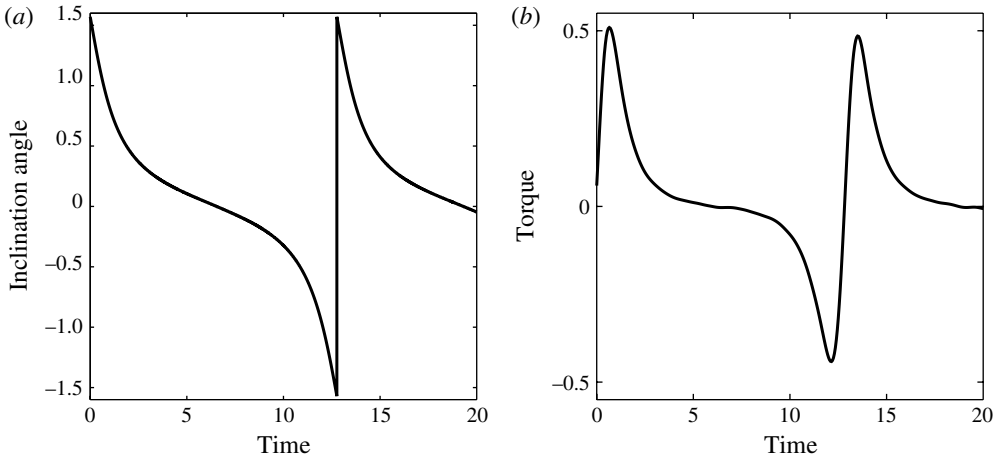

FIGURE 18. (*a*) Inclination angle and (*b*) torque of a vesicle with $\nu = 0.7$ and $\eta = 10$ in a flow for $Re = 0.1$.

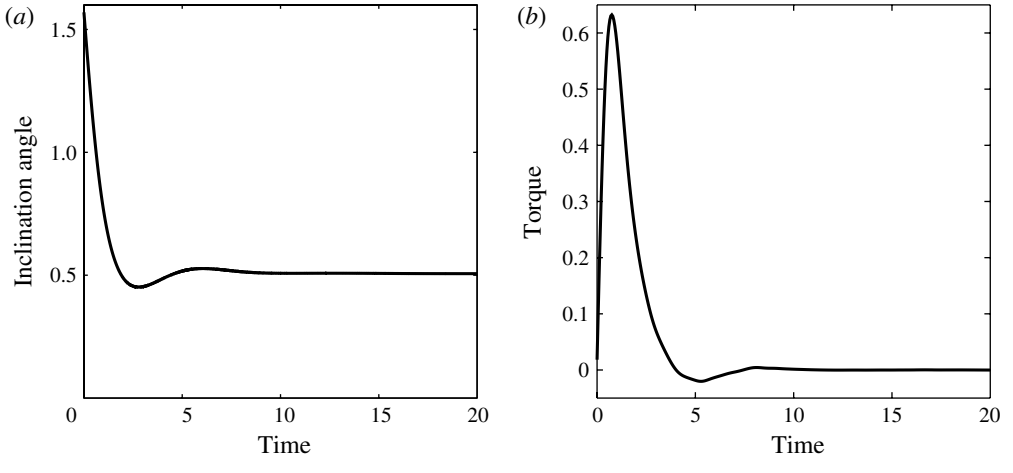

FIGURE 19. (*a*) Inclination angle and (*b*) torque of a vesicle with $\nu = 0.7$ and $\eta = 10$ in a flow for $Re = 5$.

angle, an external force must be applied. To demonstrate the overall torque acting on a vesicle, the total torque needed to fix a vesicle at a particular inclination angle has been determined. An additional external force of the form $F_\tau = -(1-H(\phi))(\boldsymbol{r}\times\boldsymbol{e}_z)T/I$, where T is the total externally applied torque and I is the moment of inertia of the vesicle, is added to (2.1). The externally applied torque is varied until the desired stable angle is achieved. Note that, while the angle is fixed, the vesicle is allowed to deform. This deformation resulted in the inability to determine the torque needed to fix a vesicle at small (near zero) and large (near $\pi/2$) inclination angles. The applied torques needed to fix a vesicle angle are shown in figure 20. This torque counters the forces on the vesicle due to the external fluid. Therefore the total torque applied to a vesicle due to the external fluid is equal to the negative of the applied torque.

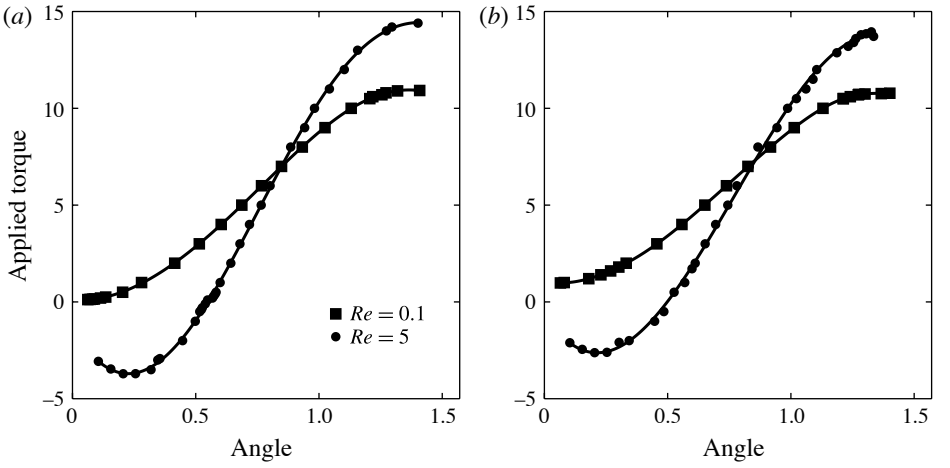

FIGURE 20. The external torque required to fix an inclination angle for vesicles with $\nu = 0.7$ and (*a*) $\eta = 5$ or (*b*) $\eta = 10$. Owing to membrane fluctuations it was not possible to fix small or large inclination angles.

It is expected that vesicles in the tumbling regime will have no zero-torque conditions, while those in the tank-treading regime will have at least one (Zettner & Yoda 2001; Mikulencack & Morris 2004). The results in figure 20 demonstrate this fact. For the shear flow characterized by $Re = 0.1$, vesicles with either viscosity ratio will tumble. In both cases the applied torque is strictly positive. The $\eta = 5$ case requires a smaller applied torque compared to the higher-viscosity-ratio case because $\eta = 5$ is closer to the initial tank-treading/tumbling critical viscosity ratio. For the higher-Reynolds-number case, $Re = 10$, vesicles with both viscosity ratios demonstrate the same zero-torque condition at approximately $\theta = 0.5$. This matches the result demonstrated in figure 17.

Rigid particles in inertial flows observe two torque-free conditions (Zettner & Yoda 2001; Mikulencack & Morris 2004). The first is the stable equilibrium angle, while the second is an unstable torque-free condition. For a flexible vesicle, it was not possible to determine the angle at which this second, unstable, torque-free condition will occur. Based on the result for the $Re = 5$ flow and the fact that the torque should be periodic with respect to inclination angle, it can be inferred that this second torque-free condition does exist.

To better understand the physical behaviour of the system at varying Reynolds numbers, the streamlines of a vesicle at a fixed angle and varying Reynolds number can be investigated (Ding & Aidun 2000). The external streamlines for a vesicle with a reduced area of $\nu = 0.7$, viscosity ratio of $\eta = 10$, fixed inclination angle of $\theta = 0.45$ and Reynolds numbers ranging from $Re = 0.1$ to $Re = 10$ are shown in figure 21. Internal streamlines are not shown, as they are qualitatively similar to those in figure 8. Figure 21 demonstrates that there are two major regimes of external fluid flow. There are shear flow layers near the walls and a recirculation region in the centre of the domain. The shear layers produce a net clockwise (negative) torque on the vesicle. This is countered by a net anticlockwise (positive) torque in the centre, recirculation region. As the Reynolds number increases, this recirculation region increases in width, resulting in an increase in the anticlockwise torque. Once the critical Reynolds number is reached, the torque in the recirculation region is able to counter the shear flow

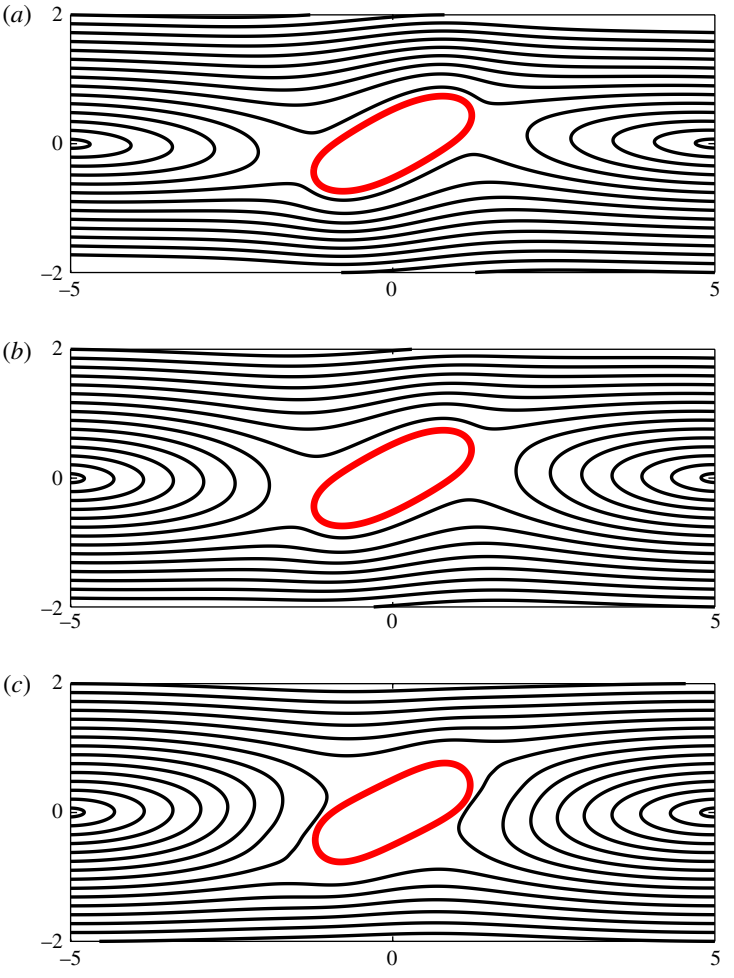

FIGURE 21. (Colour online) The streamlines for a vesicle with $\nu = 0.7$, $\eta = 10$, at a fixed angle $\theta = 0.45$ for various Reynolds number shear flows: (*a*) $Re = 0.1$; (*b*) $Re = 1$; (*c*) $Re = 10$. All cases demonstrate two regimes of fluid flow: a shear layer near the moving walls and a recirculation layer in the centre of the domain. The shear layer produces a clockwise (negative) torque, while the recirculation layer produces an anticlockwise (positive) torque.

torque, and thus the vesicle will reach a stable inclination angle. If the flow is at an elevated Reynolds number and the vesicle is below the equilibrium angle, a larger portion of the vesicle is exposed to the recirculation region. This produces a net torque that drives the vesicle to the equilibrium angle.

6.2. *Maximum tension on the membrane*

One aspect that has not yet been discussed in detail is the tension on the interface. It has been observed both experimentally (Sandre, Moreaux & Brochard-Wyart 1999) and theoretically (Tieleman *et al.* 2003; Farago & Santangelo 2005; Wang & Frenkel 2005) that the stretching of a vesicle interface will result in the formation of pores. Depending on the physical conditions, these pores may be unstable and periodically

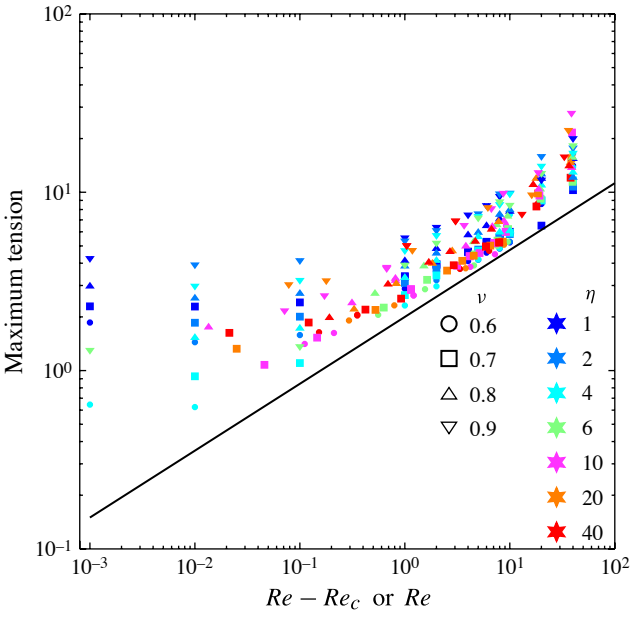

FIGURE 22. (Colour online) Log–log plot of the maximum tension on the interface during tank-treading as a function of $Re - Re_c$, where Re_c is the critical Reynolds number for the tumbling to tank-treading transition if $\eta > \eta_c$ and $Re_c = 0$ if $\eta < \eta_c$. The symbol shapes indicate the reduced area, ν, of the vesicle, while the colours represent the viscosity ratio, η. The solid line corresponds to a scaling of $(Re - Re_c)^{3/8}$.

occurring (Sandre *et al.* 1999) or stable (Farago & Santangelo 2005). Vesicles have been proposed as possible drug delivery systems (Choon & Cullis 1995; Allen & Cullis 2004; Torchilin 2006). During use as a drug delivery system, a vesicle could experience all of the conditions in the circulatory system many times over. In certain parts of the human circulatory system the effect of inertia cannot be ignored (Ku *et al.* 1985), or inertial effects can be introduced by way of restricted arteries (Bark & Ku 2010) or mechanical circulatory aids (Fraser *et al.* 2011).

The results herein have demonstrated that in inertial flows a vesicle will tank-tread with an equilibrium inclination angle dependent on the Reynolds number. As the Reynolds number increases, the inclination angle increases until a saturation angle is achieved. It was also demonstrated that, despite this change in inclination angle, the overall deformation of a vesicle does not change with an increase in inertia. For this to be possible, a corresponding increase in the tension must occur to enforce the constant-surface-area constraint and the constant deformed shape. In this model the tension varies on the membrane to account for the local velocity field. To demonstrate the change in the tension, figure 22 reports the maximum tension seen on the vesicle membrane for various tank-treading vesicles. For a given Reynolds-number flow, a vesicle with a lower viscosity ratio will have a higher tension compared to those vesicles with higher viscosity ratios. Compared to higher-viscosity encapsulated fluids, the lower-viscosity fluids apply less drag on the flow field. This results in an increase in the tank-treading velocity on the interface and thus requires an increase in the tension. For a given viscosity ratio, the maximum tension on the interface is found to increase as inertial effects increase.

It is also observed that the maximum tension on the membrane scales as

$$\gamma_{max} \propto (Re - Re_c)^{3/8} \tag{6.2}$$

regardless of the viscosity ratio. This scaling is particularly prevalent when the equilibrium angle saturates at the maximum value, which occurs for $Re > Re_c + 5$. This tension increase could become an issue for a poorly designed vesicle-based drug delivery system. A drug may be accidentally released during high inertia flows, which lowers the effectiveness of the drug or may cause serious side effects.

7. Conclusion

Here, an improved level-set based model of inertial vesicles is used to investigate the influence of the inertia on the behaviour of vesicles in simple shear flows. For viscous flows there exists a viscosity ratio below which the vesicle will tank-tread. If the viscosity ratio is increased, the vesicle will begin to tumble end over end. In inertial flows there exists a critical Reynolds number for which a vesicle will transition from the tumbling regime back to the tank-treading regime. Numerical evidence suggests that only moderate Reynolds numbers, below $Re = 10$, will suppress the tumbling of vesicles with viscosity ratios as high as 200. A systematic investigation has shown that, as the reduced area of a two-dimensional vesicle increases, the critical Reynolds number also increases. Additionally, an increase in inertial effects resulted in the equilibrium inclination angle of a vesicle increasing. Scaling laws for the tumbling period, critical Reynolds number, equilibrium angle and maximum tension on the interface are shown.

This tumbling to tank-treading transition was explored by considering the total torque applied on the vesicle due to the flow field. It was calculated that, during tank-treading inertial flows, a torque-free condition exists that corresponds to the equilibrium condition determined. The influence of Reynolds number on the tension of the vesicle membrane was also considered. As the Reynolds number increases, the tension rises. This could become an issue if the tension reaches the lysis tension, a level where poration could occur.

To further explore the influence of inertia, future work will be to investigate three-dimensional vesicles in inertial flows. The additional freedom given by the higher dimensionality may result in additional modes of vesicle behaviour. Using the results presented here and that of rigid particles (Zettner & Yoda 2001), work is under way to experimentally explore inertial effects on vesicles.

Acknowledgements

D.S. was supported by the University at Buffalo SUNY. M.J.M. was supported by NSF RTG grant DMS-0630574 and NSF grant DMS-0616468.

REFERENCES

ABKARIAN, M., FAIVRE, M. & VIALLAT, A. 2007 Swinging of red blood cells under shear flow. *Phys. Rev. Lett.* **98** (18), 188302.

ABKARIAN, M., LARTIGUE, C. & VIALLAT, A. 2002 Tank treading and unbinding of deformable vesicles in shear flow: determination of the lift force. *Phys. Rev. Lett.* **88** (6), 068103.

ABKARIAN, M. & VIALLAT, A. 2005 Dynamics of vesicles in a wall-bounded shear flow. *Biophys. J.* **89** (2), 1055–1066.

ABKARIAN, M. & VIALLAT, A. 2008 Vesicles and red blood cells in shear flow. *Soft Matt.* **4** (4), 653–657.

ALLEN, T. M. & CULLIS, P. R. 2004 Drug delivery systems: entering the mainstream. *Science* **303** (5665), 1818–1822.

BARK, D. L. & KU, D. N. 2010 Wall shear over high degree stenoses pertinent to atherothrombosis. *J. Biomech.* **43** (15), 2970–2977.

BROWN, D. L., CORTEZ, R. & MINION, M. L. 2001 Accurate projection methods for the incompressible Navier–Stokes equations. *J. Comput. Phys.* **168** (2), 464–499.

CHOON, A. & CULLIS, P. R. 1995 Recent advances in liposomal drug-delivery systems. *Curr. Opin. Biotechnol.* **6** (6), 698–708.

COUPIER, G., KAOUI, B., PODGORSKI, T. & MISBAH, C. 2008 Noninertial lateral migration of vesicles in bounded Poiseuille flow. *Phys. Fluids* **20** (11), 111702.

DANKER, G., VLAHOVSKA, P. M. & MISBAH, C. 2009 Vesicles in Poiseuille flow. *Phys. Rev. Lett.* **102** (14), 148102.

DESCHAMPS, J., KANTSLER, V., SEGRE, E. & STEINBERG, V. 2009*a* Dynamics of a vesicle in general flow. *Proc. Natl Acad. Sci. USA* **106** (28), 11444–11447.

DESCHAMPS, J., KANTSLER, V. & STEINBERG, V. 2009*b* Phase diagram of single vesicle dynamical states in shear flow. *Phys. Rev. Lett.* **102** (11), 118105.

DING, E. J. & AIDUN, C. K. 2000 The dynamics and scaling law for particles suspended in shear flow with inertia. *J. Fluid Mech.* **423**, 317–344.

DU, Q., LIU, C., RYHAM, R. & WANG, X. 2009 Energetic variational approaches in modelling vesicle and fluid interactions. *Physica* D: *Nonlinear Phenom.* **238**, 923–930.

DU, Q., LIU, C. & WANG, X. 2006 Simulating the deformation of vesicle membranes under elastic bending energy in three dimensions. *J. Comput. Phys.* **212** (2), 757–777.

DU, Q. & ZHANG, J. 2008 Adaptive finite element method for a phase field bending elasticity model of vesicle membrane deformations. *SIAM J. Sci. Comput.* **30** (3), 1634–1657.

FARAGO, O. & SANTANGELO, C. D. 2005 Pore formation in fluctuating membranes. *J. Chem. Phys.* **122**, 044901.

FRASER, K. H., TASKIN, M. E., GRIFFITH, B. P. & WU, Z. J. 2011 The use of computational fluid dynamics in the development of ventricular assist devices. *Med. Engng Phys.* **33** (3), 263–280.

FUNG, Y. C. & ZWEIFACH, B. W. 1971 Microcirculation – mechanics of blood flow in capillaries. *Annu. Rev. Fluid Mech.* **3**, 189–210.

GHIGLIOTTI, G., BIBEN, T. & MISBAH, C. 2010 Rheology of a dilute two-dimensional suspension of vesicles. *J. Fluid Mech.* **653**, 489–518.

HEILMANN, C., GEISEN, U., BENK, C., BERCHTOLD-HERZ, M., TRUMMER, G., SCHLENSAK, C., ZIEGER, B. & BEYERSDORF, F. 2009 Haemolysis in patients with ventricular assist devices: major differences between systems. *Eur. J. Cardio-thoracic Surg.* **36** (3), 580–584.

KANTSLER, V. & STEINBERG, V. 2005 Orientation and dynamics of a vesicle in tank-treading motion in shear flow. *Phys. Rev. Lett.* **95**, 258101.

KANTSLER, V. & STEINBERG, V. 2006 Transition to tumbling and two regimes of tumbling motion of a vesicle in shear flow. *Phys. Rev. Lett.* **96** (3), 036001.

KELLER, S. R. & SKALAK, R. 1982 Motion of a tank-treading ellipsoidal particle in a shear-flow. *J. Fluid Mech.* **120**, 27–47.

KRAUS, M., WINTZ, W., SEIFERT, U. & LIPOWSKY, R. 1996 Fluid vesicles in shear flow. *Phys. Rev. Lett.* **77** (17), 3685–3688.

KU, D. N., GIDDENS, D. P., ZARINS, C. K. & GLAGOV, S. 1985 Pulsatile flow and atherosclerosis in the human carotid bifurcation – positive correlation between plaque location and low and oscillating shear-stress. *Arteriosclerosis* **5** (3), 293–302.

LAADHARI, A., SARAMITO, P. & MISBAH, C. 2012 Vesicle tumbling inhibited by inertia. *Phys. Fluids* **24** (3), 031901.

LEBEDEV, V. V., TURITSYN, K. S. & VERGELES, S. S. 2008 Nearly spherical vesicles in an external flow. *New J. Phys.* **10**, 043044.

LICHTENBERG, A. J. & LIEBERMAN, M. A. 1992 *Regular and Chaotic Dynamics*. Springer.

MIKULENCACK, D. R. & MORRIS, J. F. 2004 Stationary shear flow around fixed and free bodies at finite Reynolds number. *J. Fluid Mech.* **520**, 215–242.

MIN, C. & GIBOU, F. 2006 A second-order accurate projection method for the incompressible Navier–Stokes equations on non-graded adaptive grids. *J. Comput. Phys.* **219** (2), 912–929.

MIN, C. & GIBOU, F. 2007 A second-order accurate level set method on non-graded adaptive Cartesian grids. *J. Comput. Phys.* **225** (1), 300–321.

MISBAH, C. 2006 Vacillating breathing and tumbling of vesicles under shear flow. *Phys. Rev. Lett.* **96** (2), 028104.

NOGUCHI, H., GOMPPER, G. & LUBENSKY, T. C. 2005 Shape transitions of fluid vesicles and red blood cells in capillary flows. *Proc. Natl Acad. Sci. USA* **102** (40), 14159–14164.

RAMANUJAN, S. & POZRIKIDIS, C. 1998 Deformation of liquid capsules enclosed by elastic membranes in simple shear flow: large deformations and the effect of fluid viscosities. *J. Fluid Mech.* **361**, 117–143.

RAND, R. P. 1964 Mechanical properties of the red cell membrane. II. Viscoelastic breakdown of the membrane. *Biophys. J.* **4**, 303–316.

SALAC, D. & MIKSIS, M. 2010 Reynolds number effects on the behaviour of lipid vesicles. In *Proceedings of the 63rd Annual Meeting of the APS Division of Fluid Dynamics*, vol. 55(16), RK.6. The American Physical Society.

SALAC, D. & MIKSIS, M. 2011 A level set projection method of lipid vesicles in general flows. *J. Comput. Phys.* **230** (22), 8192–8215.

SANDRE, O., MOREAUX, L. & BROCHARD-WYART, F. 1999 Dynamics of transient pores in stretched vesicles. *Proc. Natl Acad. Sci.* **96** (19), 10591–10596.

SCHWALBE, J. T., VLAHOVSKA, P. M. & MIKSIS, M. J. 2010 Monolayer slip effects on the dynamics of a lipid bilayer vesicle in a viscous flow. *J. Fluid Mech.* **647**, 403–419.

SEIFERT, U. 1997 Dynamics of giant vesicles. *Mol. Cryst. Liq. Cryst. Sci. Technol.* A – *Mol. Cryst. Liq. Cryst.* **292**, 213–225.

SEIFERT, U. 1999 Fluid membranes in hydrodynamic flow fields: formalism and an application to fluctuating quasispherical vesicles in shear flow. *Eur. Phys. J.* B **8** (3), 405–415.

SIEGENTHALER, M. P., MARTIN, J., VAN DE LOO, A., DOENST, T., BOTHE, W. & BEYERSDORF, F. 2002 Implantation of the permanent Jarvik-2000 left ventricular assist device – a single-centre experience. *J. Am. College Cardiol.* **39** (11), 1764–1772.

STRONY, J., BEAUDOIN, A., BRANDS, D. & ADELMAN, B. 1993 Analysis of shear-stress and hemodynamic factors in a model of coronary-artery stenosis and thrombosis. *Am. J. Physiol.* **265** (5, Part 2), H1787–H1796.

TANGELDER, G. J., SLAAF, D. W., ARTS, T. & RENEMAN, R. S. 1988 Wall shear rate in arterioles in vivo – least estimates from platelet velocity profiles. *Am. J. Physiol.* **254** (6, Part 2), H1059–H1064.

TIELEMAN, D. P., LEONTIADOU, H., MARK, A. E. & MARRINK, S. J. 2003 Simulation of pore formation in lipid bilayers by mechanical stress and electric fields. *J. Am. Chem. Soc.* **125** (21), 6382–6383.

TORCHILIN, V. P. 2006 Multifunctional nanocarriers. *Adv. Drug Deliv. Rev.* **58** (14), 1532–1555.

VEERAPANENI, S. K., GUEYFFIER, D., BIROS, G. & ZORIN, D. 2009*a* A numerical method for simulating the dynamics of 3D axisymmetric vesicles suspended in viscous flows. *J. Comput. Phys.* **228** (19), 7233–7249.

VEERAPANENI, S. K., GUEYFFIER, D., ZORIN, D. & BIROS, G. 2009*b* A boundary integral method for simulating the dynamics of inextensible vesicles suspended in a viscous fluid in 2D. *J. Comput. Phys.* **228** (7), 2334–2353.

VLAHOVSKA, P. M. & GRACIA, R. S. 2007 Dynamics of a viscous vesicle in linear flows. *Phys. Rev.* E **75** (1), 016313.

VLAHOVSKA, P. M., PODGORSKI, T. & MISBAH, C. 2009 Vesicles and red blood cells in flow: from individual dynamics to rheology. *C. R. Phys.* **10** (8), 775–789.

WANG, Z. J. & FRENKEL, D. 2005 Pore nucleation in mechanically stretched bilayer membranes. *J. Chem. Phys.* **123**, 154701.

XIU, D. B. & KARNIADAKIS, G. E. 2001 A semi-Lagrangian high-order method for Navier–Stokes equations. *J. Comput. Phys.* **172** (2), 658–684.

ZABUSKY, N. J., SEGRE, E., DESCHAMPS, J., KANTSLER, V. & STEINBERG, V. 2011 Dynamics of vesicles in shear and rotational flows: modal dynamics and phase diagram. *Phys. Fluids* **23** (4), 041905.

ZETTNER, C. M. & YODA, M. 2001 Moderate-aspect-ratio elliptical cylinders in simple shear with inertia. *J. Fluid Mech.* **442**, 241–266.

ZHAO, R., ANTAKI, J. F., NAIK, T., BACHMAN, T. N., KAMENEVA, M. V. & WU, Z. J. 2006 Microscopic investigation of erythrocyte deformation dynamics. *Biorheology* **43** (6), 747–765.

ZHAO, H. & SHAQFEH, E. S. G. 2009 The dynamics of a vesicle in shear flow. *Tech. Rep*. Stanford University.

ZHAO, H. & SHAQFEH, E. S. G. 2011 The dynamics of a vesicle in simple shear flow. *J. Fluid Mech.* **674** (1), 578–604.